

High-resolution two-proton stripping to $2p-1h$ $7/2^-$ states via the $^{59}\text{Co}(^3\text{He},n\gamma)^{61}\text{Cu}$ reaction

P. Papka^{1,2,a}, J.F. Sharpey-Schafer³, B.A. Brown⁴, T.S. Dinoko³, E.A.M.A. Khaleel¹, E.A. Lawrie², J.J. Lawrie², K.C.W. Li¹, S.N.T. Majola², W.A. Richter^{2,3}, O. Shirinda^{2,3}, M.A. Stankiewicz⁵, P. Vymers¹, and M. Wiedeking²

¹ Department of Physics, University of Stellenbosch, Private Bag X1, 7602 Matieland, South Africa

² iThemba LABS, National Research Foundation, PO Box 722, Somerset West 7129, South Africa

³ Department of Physics, University of the Western Cape, Bellville ZA-7535, South Africa

⁴ Department of Physics and Astronomy and National Superconducting Cyclotron Laboratory, Michigan State University East Lansing, Michigan 48824-1321, USA

⁵ Department of Physics, University of Cape Town, Rondebosch 7700, South Africa

Received: 16 September 2014

Published online: 28 October 2014 – © Società Italiana di Fisica / Springer-Verlag 2014

Communicated by H. Miyatake

Abstract. The challenge of achieving high resolution in binary reactions involving an outgoing high-energy neutron is solved by detecting the γ -ray decay of populated excited states in an array of escape-suppressed HPGe detectors in coincidence with fast neutrons. The selectivity of the arrangement is of the order of 1 in 1000 and is demonstrated by $L = 0$ two-proton stripping to $7/2^-$ $2p-1h$ levels using the $^{59}\text{Co}(^3\text{He},n\gamma)^{61}\text{Cu}$ reaction at $E_{\text{lab}} = 22.5$ MeV. The observed relative two-proton stripping strengths are compared with large-basis shell-model calculations.

1 Introduction

The challenge of detecting outgoing high-energy neutrons from binary reactions with excellent energy resolution, together with high efficiency, has not been satisfactorily achieved. The (d, n) single proton stripping reaction can be proxied by the surrogate $(^3\text{He}, d)$ reaction. However, the Distorted Wave Born Approximation (DWBA) theory of $(^3\text{He}, d)$ reactions relies on some approximations due to momentum mismatch and the internal structures of the ^3He and deuteron [1]. This adds uncertainty in being able to adequately derive spectroscopic factors from the data. Analysis of (d, n) data would be much more straightforward but experimental time-of-flight (t-o-f) energy resolutions for the fast direct reaction neutrons are usually measured in hundreds of keV. For two-proton stripping there is no surrogate for the $(^3\text{He}, n)$ reaction. As reviewed in ref. [2], heavy-ion reactions can be used, such as with ^{12}C , ^{16}O or even heavier projectiles, but the cross-sections are smaller than for light-ion direct reactions. Besides this, it is still difficult to achieve good energy resolutions due to energy losses in the targets and, again, the internal structures of the heavy ions complicate the interpretation of the data [3].

Two-neutron stripping data from (t, p) reactions have provided considerable valuable information on the paired neutron component of the configurations of the excited states of many nuclei. This has been particularly productive in assisting the understanding of pairing forces in both spherical and deformed nuclei [4]. However, there is a paucity of accurate experimental information on paired proton components of wave functions. High resolution data using the simplest of two-proton stripping reactions, the $(^3\text{He}, n)$ reaction, is highly desirable. In this paper we show that this objective can be realized by using an escape-suppressed array of HPGe γ -ray detectors in coincidence with a wall of neutron detectors placed at forward angles. We demonstrate the selectivity of the apparatus using the $^{59}\text{Co}(^3\text{He}, n\gamma)^{61}\text{Cu}$ reaction and compare the results to the predictions of shell-model calculations in the fp basis.

2 Experimental arrangement

The outgoing particles from direct reactions are peaked in the forward direction, the peak of the angular distribution being characteristic of the transferred orbital angular momentum L [5]. This peak angle increases as L increases. Thus, in (t, p) reactions, the angular distribution

^a e-mail: papka@sun.ac.za

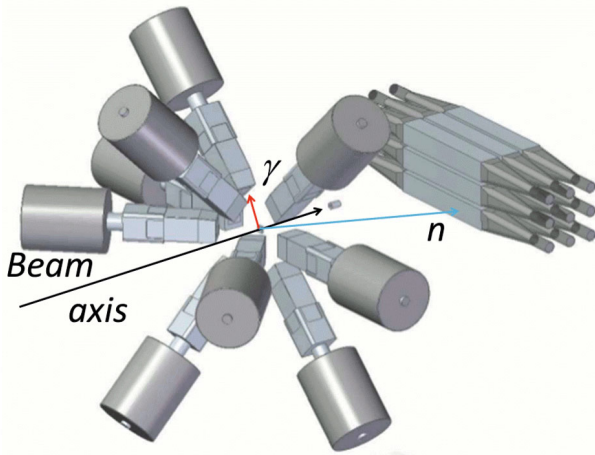


Fig. 1. Schematic diagram of the experimental setup. The AFRODITE γ -ray spectrometer consists of 9 HPGe clover detectors in BGO shields, 5 were at $\theta_{\text{lab}} = 90^\circ$ and 4 at $\theta_{\text{lab}} = 135^\circ$ with respect to the beam direction. The neutron detectors were arranged in three walls of three detectors placed at 0° .

of the outgoing proton that peaks at a scattering angle of $\theta_{\text{lab}} = 0^\circ$ has $L = 0$. Hence, in this case, as no angular momentum is transferred, the spin of the final state must equal that of the target nucleus. The same is true for the $(^3\text{He}, n)$ two-proton stripping reaction. Clearly, these reactions are very useful for unambiguously identifying simple configurations in nuclei, especially excited 0^+ states such as those observed in double- β decay [6, 7].

The feasibility of using escape-suppressed arrays of γ -ray detectors in coincidence with charged particles emitted in direct reactions has been demonstrated on many occasions, for example, at Berkeley National Laboratory by Allmond *et al.* [8]. Numerous n - γ coincident measurements have also been performed using t-o-f and/or pulse shape analysis discrimination methods such as with the EUROBALL-Neutron wall experimental setup [9]. The $(^3\text{He}, n)$ reaction generally has high positive Q -values ranging between 0 and 10 MeV. Thus, for 20 MeV beams of ^3He , the direct reaction neutrons will have energies between 20 and 30 MeV. This is in contrast to the competing statistical neutrons from the $(^3\text{He}, xn)$ fusion-evaporation reactions which have energies peaking at about 2 MeV with a distribution falling exponentially at higher energies. As the velocity of the neutrons is proportional to the square root of their energy, $\sqrt{E_n}$, it follows that the direct reaction neutrons have more than three times the velocity of the bulk of statistical neutrons and may be separated by t-o-f measurement over relatively short distances of $d \approx 2$ m. The γ -rays from the reaction can be blocked from the neutron detectors by Pb absorbers without materially affecting the detection of fast neutrons. This obviates the necessity of using neutron detectors that discriminate between neutrons and γ -rays.

As $L = 0$ transitions are peaked at $\theta_{\text{lab}} = 0^\circ$, neutron detectors placed downstream of the target will intersect the majority of the $L = 0$ neutrons, preferentially selecting

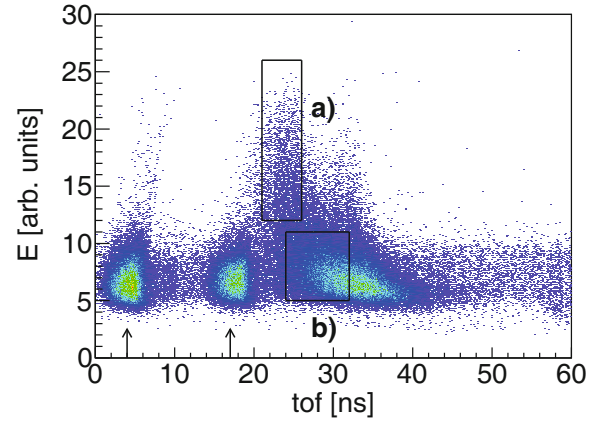


Fig. 2. Two-dimensional scatterplot of the energy E deposited in a scintillator (pulse height) versus t-o-f. The two gates indicated as (a) and (b) select the fast neutrons and statistical neutrons, respectively. Gate (b) is used for background subtraction of the predominant $^{59}\text{Co}(^3\text{He}, pn)^{60}\text{Ni}$ fusion evaporation reaction. The two arrows at 4 ns and 17 ns indicate the loci of the γ -rays originating from the target and beam dump, respectively. A high-energy threshold placed at the time of the measurement discarded most of the low energy γ -rays and statistical neutrons.

states with the same spin as the target. Neutron detectors at angles significantly away from $\theta_{\text{lab}} = 0^\circ$ would pick up higher L values and other states. One extra advantage of this experimental arrangement is that relatively thick targets may be used as the high resolution originates from the γ -rays and not from the neutrons.

Our apparatus is shown schematically in fig. 1. In this experiment, a ^{59}Co target of thickness 9.6 mg/cm^2 was bombarded by a ^3He beam of $E_{\text{lab}} = 22.5 \text{ MeV}$ incident energy and intensity of the order of 0.65 pA from the iThemba LABS Separated Sector Cyclotron (SSC). The target was placed at the center of the AFRODITE escape-suppressed spectrometer [10] and the beam was stopped in a lead cup placed between the target (0.5 m downstream) and the neutron detectors. HPGe Clover detectors in BGO shields were positioned at $\theta_{\text{lab}} = 135^\circ$ (4 detectors) and at $\theta_{\text{lab}} = 90^\circ$ (5 detectors) with respect to the beam direction.

The count rate using a γn trigger varied between 50 and 200 Hz for a total beam exposure of $2.61 \times 10^4 \text{ s}$. Analogue electronics was used and with such low count rate the dead time was negligible. Time-to-amplitude converters were used to measure the time difference between the cyclotron reference and the signal from the neutron detectors.

The neutron detectors consisted of a set of 9 large-volume NE102A plastic scintillators $0.6 \times 0.1 \times 0.1 \text{ m}^3$ each, with no particle discrimination capability, initially built for the neutron t-o-f setup at iThemba LABS [11]. These detectors were placed symmetrically about $\theta_{\text{lab}} = 0^\circ$ and perpendicular to the beam, downstream of the target. Scintillations from the detectors are viewed at either end by Hamamatsu R329 photomultipliers. The relative amplitude between the signals of the PMTs allows the neu-

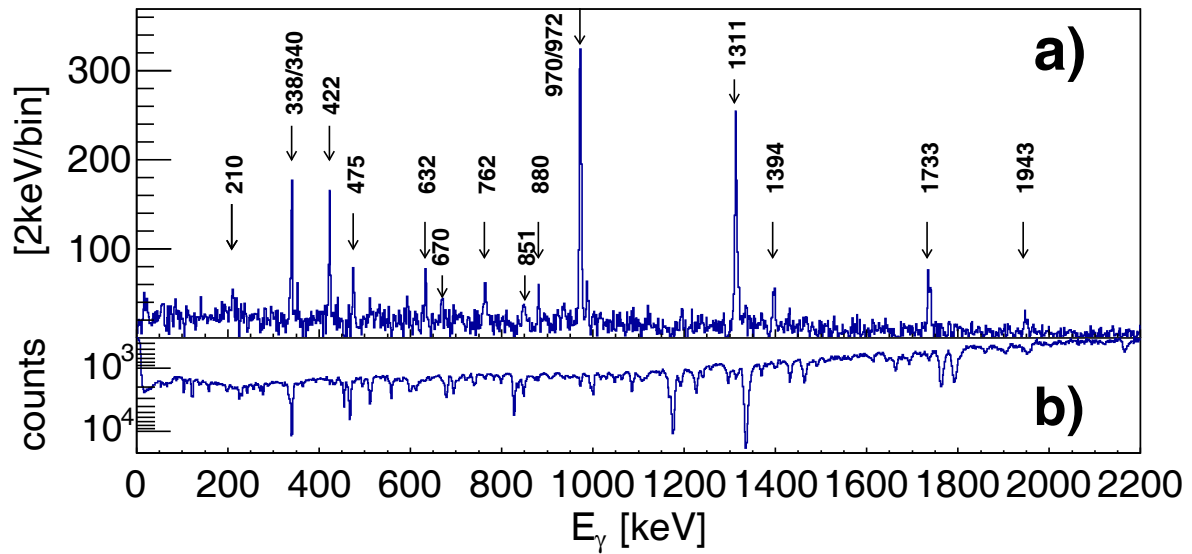


Fig. 3. γ -ray spectra from the $^{59}\text{Co}(^3\text{He}, n\gamma)^{61}\text{Cu}$ reaction. Spectrum (a) contains γ -rays in coincidence with fast neutrons gated as illustrated in fig. 2 and spectrum (b) ungated γ -rays. The gated spectrum contains almost exclusively γ -ray transitions from ^{61}Cu (indicated with arrows).

tron detection to be located with an uncertainty of 50 mm within their 600 mm length. The detectors were placed 1.5 m from the target and arranged in a 3×3 compact geometry. Three vertical walls of three detectors placed on top of each other presented a total effective thickness of 0.3 m. The $^{59}\text{Co}(^3\text{He}, n)^{61}\text{Cu}$ reaction has a positive Q -value of 6.606 MeV so that the outgoing neutron carries an energy larger than the beam energy. Large energy deposition in the detectors together with the t-o-f measurement are used to identify fast neutrons as illustrated in the contour plot of fig. 2. The time between two selected beam pulses from the SSC was 360 ns. Such selection allows fusion evaporation events to be discriminated against. The neutrons from fusion-evaporation are produced with typical cross-sections of 0.6 b (PACE4 calculation) compared to sub mb cross-section for the direct $(^3\text{He}, n)$ reaction.

The 9 neutron detectors cover a solid angle of 0.15 sr. Fast neutrons are selected in the successive layers with a light output selection corresponding to an energy deposition larger than $E > 12$ MeV. The data is for single hits in the neutron wall and the double hits, where neutrons have scattered from one scintillator to another, are rejected. A full simulation of the experimental setup was performed using the GEANT4 toolkit [12] together with the CADmesh interface [13]. The simulations were performed with the high-precision QGSP_BERT_HP physics list in order to estimate the amount of fast neutrons depositing only a small part of their energy and falling in the statistical neutron region partly selected within gate (b) of fig. 2. It is found that 34% of the fast neutrons impinging on the neutron wall deposit an energy larger than $E > 12$ MeV.

The angular distribution of the γ -rays originating from the $7/2^-$ states is expected to be isotropic due to $L = 0$ angular momentum transfer. This is verified for the strongest

1311 keV transition in ^{61}Cu . Based on the AFRODITE total efficiency, measured using a standard ^{56}Co source to cover up to 3.5 MeV of the energy range, cross-sections can be estimated. States in ^{61}Cu are populated with cross-sections up to 0.4 mb/sr for the strongest state at 1311 keV ($\theta_{\text{lab}} < 15^\circ$). This is consistent with a total $(^3\text{He}, n)$ cross-section of 6.4 mb reported in ref. [14] for a center of target energy of 21 MeV. Note that the states fed through $L > 0$ are observed very weakly as most of the cross section is expected to be found for larger θ angles for which the current setup is insensitive.

The spectra of fig. 3 show the high rejection factor of the main fusion-evaporation channels visible in fig. 3(b) with a signal-to-background ratio improved by a factor of nearly 1000 for the strongest ^{61}Cu transitions. The largest peaks in this background spectrum come from the $^{59}\text{Co}(^3\text{He}, pn)^{60}\text{Ni}$ reaction. These evaporation channels are dramatically reduced in the fast neutron gated spectrum of fig. 3(a) where the γ -rays from the lowest three $7/2^-$ levels in ^{61}Cu can clearly be identified. Detection of the fast neutrons near $\theta_{\text{lab}} = 0^\circ$ reduces the probability of detecting neutrons emitted isotropically by statistical processes enhancing the signal from direct reaction neutrons. The states populated through low angular momentum transfer decay via a small number of transitions depending on the spin and parity of the final ground state (see fig. 4). With such low multiplicity γ - γ coincidences are ineffective as verified by constructing γ - γ matrices.

3 Results and discussion

The known branching ratios from *Data Tables* [15] and from ref. [16] were used to deduce the feeding of the states. The strengths are normalized to the strongest transition from the lowest $7/2^-$ state at 1311 keV (see fig. 3(a)).

Table 1. Relative population strengths Γ , normalized to the 1311 keV strength set as 100, and branching ratios of the $7/2^-$ states in ^{61}Cu populated in the $^{59}\text{Co}(^3\text{He}, n)^{61}\text{Cu}$ reaction. The calculated population strengths are based on the large-basis shell model, NuShellX [18–21], calculations.

J^π	E_x [keV]	E_γ [keV]	Branching %		Γ		Proton occupation w.r.t. full $f_{7/2}$			
			Data tables	Theory SM	Data	SM	$0f_{7/2}$	$1p_{3/2}$	$1p_{1/2}$	$0f_{5/2}$
$7/2^-$	1310.5	340.2	6.2	5	100	100	-0.74	1.32	0.20	0.22
		1310.5	93.8	95						
$7/2^-$	1732.6	338.4	2.3	6	68(14)	190	-0.78	1.29	0.23	0.26
		421.8	22.3	61						
		762.4	13.6	27						
		1732.7	61.8	6						
$7/2^-$	1942.5	209.6	10.0	27	115(30)	470	-1.16	1.45	0.34	0.38
		548.0	0.5	2						
		631.9	19.2	28						
		972.4	60.0	35						
		1942.8	10.3	8						

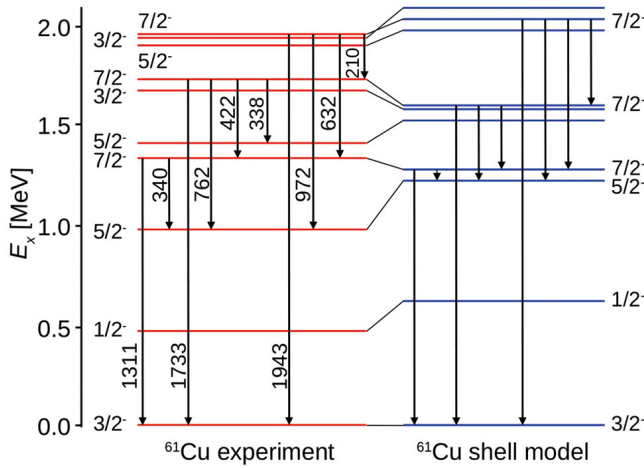


Fig. 4. Experimentally established levels in ^{61}Cu [15] below 2.0 MeV excitation energy compared with shell-model calculations in the $0f_{7/2}$, $1p_{3/2}$, $1p_{1/2}$ and $0f_{5/2}$ basis. The labeled γ -rays are those observed from $7/2^-$ states in the present experiment, as shown in fig. 3.

The relative population strengths of the $7/2^-$ states in ^{61}Cu extracted from this work are given in table 1. The transitions identified in this reaction are shown in the partial level scheme of fig. 4 together with the location of the excited states from the shell-model (SM) calculations.

The calculations were carried with NuShellX [17] in the pf shell model space with the GPFX1A Hamiltonian [18–21]. Some truncation had to be made in terms of the configurations [proton $(0f_{7/2})^{f_p} (0f_{5/2}, 1p_{3/2}, 1p_{1/2})^{r_p}$] [neutron $(0f_{7/2})^{f_n} (0f_{5/2}, 1p_{3/2}, 1p_{1/2})^{r_n}$]. The largest dimension that could possibly be used for ^{61}Cu was with $f_p = (4, 8)$, $r_p = (1, 5)$, $f_n = (6, 8)$, $r_n = (4, 6)$, where the numbers are the minimum and maximum allowed in each group of orbitals. In this specific case the M-scheme dimension was 761, 643, 757.

The energies are compared with experiment in fig. 4. The γ -decay was calculated with $M1$ and $E2$ effective operators obtained from fits to sd shell data with wave functions obtained with the USDA Hamiltonian [22]. Harmonic-oscillator radial wave functions with $\hbar\omega = 9.82$ MeV were used. The calculated branching ratios are compared with experiment in table 1. For the γ -decay phase space factors the experimental energies were used. The largest deviation between calculations and experiment is found for the branching of the $(7/2^-)_2$ state to the ground state; 62% observed *vs.* 6% calculated. The reason may be due to the very hindered $E2$ strength in the calculation for this transition corresponding to 1.0×10^{-3} W.u. The sensitivity to the Hamiltonian needs to be investigated. From calculations, the configuration of the states is clearly dominated by a pair of protons in the $1p_{3/2}$ orbital with a hole in the $f_{7/2}$ shell. The three $7/2^-$ states under $E_x < 1943$ keV are consequently strongly populated by transferring an antialigned pair of protons from the incoming projectile to the ^{59}Co core. The two $7/2^-$ states at 2399 and 2728 keV are weakly populated. This is consistent with calculations, indicating a $(1p1h)$ excitation resulting in a lower two-proton occupation of the $1p_{1/2}$ orbital and increased occupation of the $1p_{3/2}$ orbital.

Two-particle transfer amplitudes (TNA) for ^{59}Co to ^{61}Cu were calculated with NuShellX. These were then used in FRESKO [23] to calculate the cross sections for $L = 0$ transfer. The calculated cross-sections at zero degrees are 43, 82 and $202 \mu\text{b}/\text{sr}$ for the first, second and third $7/2^-$ states, respectively. The higher energy $7/2^-$ states have lower cross-sections ($< 10 \mu\text{b}/\text{sr}$). The relative cross-sections of 100, 190 and 470 (normalized to the 1311 keV strength set as 100) calculated with the shell model are not in very good agreement with experiment (see table 1). However, the qualitative result that the lowest three $7/2^-$ states are predominantly populated is reproduced. From calculations, the population of higher energy $7/2^-$ states starting with the fourth one at 2399 keV (predicted at 2471 keV) is an order of magnitude smaller than the lowest three, in agreement with experiment.

4 Conclusion

The challenge in achieving high resolution measurements using ($^3\text{He}, n$) reactions is addressed by combining a γ -ray spectrometer together with a neutron detector array placed at small angles using the $^{59}\text{Co}(^3\text{He}, n)^{61}\text{Cu}$ reaction. States with $L = 0$ momentum transfer were populated very selectively and excellent signal-to-background ratio was achieved. The first three $7/2^-$ states of ^{61}Cu are strongly populated by two proton transfer relative to other known excited states. The shell model calculations predict that all three of these states have the $1p_{3/2}$ orbital having most of the two-proton, one-proton hole strength. However, the full fp shell model does not give a good account of the relative strengths of the two proton stripping to these three states. A very simple model, where the target ^{59}Co has a pure one proton hole in the $1f_{7/2}$ shell and the stripped pair of protons going into $2p_{3/2}$, $2p_{1/2}$ and $1f_{5/2}$ orbits, would give a ratio of intensities proportional to $(2j + 1)$ where j is the spin of the single proton orbit outside ^{60}Ni . This gives a ratio of 4 : 2 : 6 or 100 : 50 : 150 compared to our measured ratio (table 1) of 100 : 68(14) : 115(30). This experiment indicates that our current shell model underestimates the shell closure at $Z = 28$. High-resolution measurement of two-proton stripping can be performed throughout the nuclear chart. Hopefully, this will lead to a much improved understanding of the influence of proton pairing in the structure of nuclei.

We wish to acknowledge the support of the Michigan State University High Performance Computing Center, the Institute for Cyber-Enabled Research and support from NSF grant PHY-1068217. This work was financially supported by the National Research Foundation of South Africa.

References

1. N.K. Glendenning, *Direct Nuclear Reactions* (Academic Press, 1983).
2. W. von Oertzen and A. Vitturi, Rep. Prog. Phys. **64**, 1247 (2001).
3. C.A. Ogilvie *et al.*, Phys. Rev. C **39**, 139 (1989).
4. D.M. Brink, R.A. Broglia, *Nuclear Superfluidity: Pairing in Finite Systems*, in *Cambridge Monographs on Particle Physics Nuclear Physics and Cosmology*, Vol. **24** (Cambridge University Press, 2005).
5. J.R. Holt, T.N. Marsham, Proc. Phys. Soc. A **66**, 1032 (1953).
6. M.J. Hornish *et al.*, Phys. Rev. C **74**, 044314 (2006).
7. A.S. Barabash *et al.*, Phys. Rev. C **79**, 045501 (2009).
8. J.M. Allmond *et al.*, Phys. Rev. C **81**, 064316 (2010).
9. Ö. Skeppsted *et al.*, Nucl. Instrum. Methods Phys. Res. A **421**, 531 (1999).
10. J.F. Sharpey-Schafer, Nucl. Phys. News Int. **14**, 5 (2004).
11. V.M. Tshivhase, PhD thesis, University of Cape Town (1997).
12. S. Agostinelli *et al.*, Nucl. Instrum. Methods A **506**, 250 (2003).
13. C.M. Poole *et al.*, Austr. Phys. Eng. Sci. Med. **35**, 329 (2012).
14. F. Szelecsényi *et al.*, Nucl. Instrum. Methods Phys. Res. B **222**, 364 (2004).
15. M.R. Bhat, Nucl. Data Sheets **88**, 417 (1999).
16. L.-L. Andersson *et al.*, Eur. Phys. J. A **36**, 251 (2008).
17. B.A. Brown, W.D.M. Rae, E. McDonald, M. Horoi, NuShellX@MSU.
18. M. Honma *et al.*, Phys. Rev. C **65**, 061301 (2002).
19. M. Honma *et al.*, Phys. Rev. C **69**, 034335 (2004).
20. www.nsc1.msu.edu/~brown/resources/resources.html.
21. W.D.M. Rae, <http://www.garsington.eclipse.co.uk/>.
22. W.A. Richter *et al.*, Phys. Rev. C **78**, 064302 (2008).
23. <http://www.fresco.org.uk/>.